Inorganica Chimica Acta 518 (2021) 120244

Contents lists available at ScienceDirect

Inorganica Chimica Acta

journal homepage: www.elsevier.com/locate/ica

Research paper

Alkyl tetrazoles as diimine ("diim") ligands for *fac*-[Re(diim)(CO)$_3$(L)]-type complexes. Synthesis, characterization and preliminary studies of the interaction with bovine serum albumin

Nicola Monti [a], Veronica Longo [a], Stefano Zacchini [a], Giulia Vigarani [a], Loris Giorgini [a], Eugenia Bonora [a,b], Massimiliano Massi [b,*], Valentina Fiorini [a,*], Stefano Stagni [a,*]

[a] Department of Industrial Chemistry "Toso Montanari", University of Bologna, Viale Risorgimento 4, I-40136 Bologna, Italy
[b] Curtin Institute for Functional Molecules and Interfaces, School of Molecular and Life Science, Curtin University, Kent Street, Bentley 6102 WA, Australia

ARTICLE INFO

Dedicated to Professor Maurizio Peruzzini on the occasion of his 65th birthday.

Keywords:
Triscarbonyl Re(I) diimine complexes
Diimine type ligands
Alkyl tetrazoles
Luminescence
Protein binding

ABSTRACT

Herein, we report a new family of luminescent Re(I) complexes with general formula ***fac*-[Re(diim)(CO)$_3$L]$^{0/+}$** in which the role of the diimine-type chelating ligand (**diim**) is played by alkylated tetrazoles. In particular, the design of the new complexes involved the choice of molecular scaffolds based on 2-pyridyl tetrazole (PTZ) and 2-quinolyl tetrazole (QTZ) which were decorated with various alkyl residues at N-2 position of the pentatomic ring, thereby endowing the resulting alkyl tetrazoles **PTZ-R** and **QTZ-R** with the proper "bpy-like" coordination attitude. As the "third" ligand (L), pyridine (**pyr**) or the 5-phenyl tetrazolato anion (**Tph**)$^-$ were selected, leading to cationic species such as ***fac*-[Re(CO)$_3$(PTZ-R)(pyr)]$^+$**, ***fac*-[Re(CO)$_3$(QTZ-R)(pyr)]$^+$** and to the neutrally charged "fully tetrazole" complex ***fac*-[Re(CO)$_3$(QTZ-Me)(Tph)]**. All the new complexes were identified by ESI-MS spectrometry and fully characterized by IR, ^{1}H and ^{13}C NMR spectroscopy. The findings that were suggested from the interpretation of the spectroscopic data were further confirmed by X-ray crystallography, with the analysis of the molecular structures of the cationic complexes ***fac*-[Re(CO)$_3$(PTZ-Me)(pyr)] [PF$_6$]** and ***fac*-[Re(CO)$_3$(QTZ-Me)(pyr)] [PF$_6$]**. Following the in-depth investigation of their photophysical properties, the new luminescent Re(I) tetrazole -based complexes were studied for any possible interaction with Bovine Serum Albumin (BSA). The results obtained from this preliminary screening highlighted that, along the series of the Re(I) tetrazole complexes, the QTZ-R based cationic derivatives ***fac*-[Re(CO)$_3$(QTZ-Me)(pyr)]$^+$**, ***fac*-[Re(CO)$_3$(QTZ-^{t}Bu)(pyr)]$^+$**, as well as the neutrally charged and "fully tetrazole" complex ***fac*-[Re(CO)$_3$(QTZ-Me)(Tph)]**, displayed the highest affinity to BSA.

1. Introduction

An "archetypal" structure like ***fac*-[Re(CO)$_3$(diim)(L)]$^{0/+}$**, where (diim) represents a bidentate aromatic diimine and (L) is a monodentate ancillary ligand, is commonly used to depict Re(I)triscarbonyl diimines, which are known as one of the most important classes of phosphorescent d^6-metal complexes that have been – and continue to be - at the centre of intense investigation in many areas of science and technology [1]. In particular, Re(I) triscarbonyl diimines have been extensively studied in the context of life science, as witnessed by the numerous reports dealing with their use as luminescent imaging for live cells and tissues and intra or extra cellular sensing agents for wide range of analytes [2,3,4]. The reasons that have driven this family of Re(I) complexes to such a biology-oriented applicative scenario are explained by their use as model compounds for the technetium-99 congeners and to their displaying a peculiar environmental sensitivity of the emission stemming from metal-to-ligand charge transfer (MLCT) excited states [5]. In particular, the structure-to-properties approach that is commonly adopted for the design of ***fac*-[Re(CO)$_3$(diim)L]$^{0/+}$** type species for bioimaging purposes relies upon the modulation of their luminescent outputs by performing chemical modifications onto the chelate diimine ligand (diim), while the biological targeting is pursued with the choice of an appropriate "third" monodentate ligand (L) [6]. Actually, the factors that govern the cellular uptake and the intracellular localization of luminescent metal complexes are yet far from being fully understood. Nevertheless, the adoption of a similar design strategy - which also

* Corresponding authors.
E-mail addresses: M.Massi@curtin.edu.au (M. Massi), valentina.fiorini5@unibo.it (V. Fiorini), stefano.stagni@unibo.it (S. Stagni).

https://doi.org/10.1016/j.ica.2020.120244
Received 21 November 2020; Received in revised form 26 December 2020; Accepted 27 December 2020
Available online 7 January 2021

included the decoration of ***fac*-[Re(CO)$_3$(diim)L]$^{0/+}$** type complexes with pendant biologically active molecules – has led to an impressively high number of reports dealing with the use of such kind of Re(I) complexes as luminescent imaging reagents, among which the mitochondria specific Re(I) cationic complex reported by Coogan and co-workers in 2012 represents one of the most successful examples [7]. In this specific context, we have dedicated intense research efforts to the design of luminescent markers for cellular imaging based on neutrally charged Re(I) complexes with general formula ***fac*-[Re(CO)$_3$(diim)(L)]$^{0/+}$**, in which the third ligand (L) was represented by variably substituted 5-aryl tetrazolato anion [R-CN_4^-]. The results obtained so far have highlighted how the nature of the residue/substituent R represented a key factor for determining any eventual localization of the corresponding Re(I) complexes, which could be directed toward lipid droplets (as in the case of 4-benzonitrile substituted tetrazolato anion) or to the endoplasmic reticulum, as was observed when the residue R was represented by the 3-pyridyl ring [8]. Aiming at getting further insights about the importance of tetrazole ligands for this class of Re(I)-based luminescent markers, we now extend our studies to the design and the preparation of series of new ***fac*-[Re(CO)$_3$(diim)(L)]$^{0/+}$** type complexes in which alkylated tetrazoles play the role of the chelating "diimine like" (diim) ligands. For this specific purpose, the 2-pyridyl (PTZ) and 2-quinolyl tetrazole (QTZ) molecular scaffolds were modified with the introduction one methyl (**PTZ-Me** and **QTZ-Me**) or one *tert*-butyl (**PTZ-^{t}Bu** and **QTZ-^{t}Bu**) substituent group in the pentatomic ring, to afford the precursor species ***fac*-[Re(CO)$_3$(PTZ-R)(Br)]** and ***fac*-[Re(CO)$_3$(QTZ-R)(Br)]**, respectively. In the successive stage, their molecular architectures was modified either by introducing pyridine as the (L) ligand, leading to the series of cationic complexes with general formula ***fac*-[Re(CO)$_3$(PTZ-R)(pyr)]$^+$** and ***fac*-[Re(CO)$_3$(QTZ-R)(pyr)]$^+$**, (Fig. 1) or with the replacement of the bromide ion with one phenyl tetrazolato anion, thereby causing the formation of "fully tetrazole" charge neutral complex ***fac*-[Re(CO)$_3$(QTZ-Me)(Tph)]** (Fig. 1). Herein, the synthesis and the spectroscopic and structural characterization of the new complexes are described, along with an in-depth analysis of their photophysical properties. In addition, continuing our recent studies dealing with the use of Re(I) tetrazole complexes as luminescent staining agents for proteins [9], the preliminary results about the investigation of any possible interaction of the new Re(I) complexes with a model protein such as bovine serum albumin (BSA) are reported.

2. Results and discussions

Since tetrazoles are commonly considered the nitrogen analogues of the corresponding carboxylic acids, the use of the pyridyl-(PTZ) and quinolyl-tetrazole (QTZ) molecular scaffold as neutral diimine type chelate ligands required the replacement of the fairly acidic hydrogen of the -CN_4H moiety with an alkyl residue, leading to the alkylated tetrazoles abbreviated as **PTZ-R** and **QTZ-R**, respectively, in which the -R group was introduced at the N-2 position of the tetrazole moiety. In doing this, the peculiar reactivity that tetrazoles display toward the addition of electrophiles had to be taken into account. Indeed, the alkylation reaction of tetrazoles usually leads to the recovery of the alkylated products as a mixture of regioisomers depending whether the electrophilic addition takes place at the N-1 or the N-2 position of the pentatomic ring [10].

As the steric hindrance of the -R group is the most important factor for determining any eventual regiospecificity of the alkylation reactions, the addition of the bulky tert-butyl (^{t}Bu) residue to 2-pyridyl tetrazole (PTZ-H) and 2-quinolyl tetrazole (QTZ-H) led to the exclusive formation of the desired N-2 tert-butylated derivatives (**PTZ-^{t}Bu**) and (**QTZ-^{t}Bu**). On the other hand, the methylation reaction performed onto the same tetrazole substrates provided the methylated compounds (**PTZ-Me**) and (**QTZ-Me**) as mixtures of both regioisomers, from which the N-2 substituted isomers were isolated following a column chromatography work up (Fig. 2 and experimental section for further details). In particular, the clear distinction of the two substitution isomers could be made from the analysis of the corresponding ^{13}C NMR spectra. In fact, whereas the resonance of the tetrazole carbon (C_t) of N-1 isomers is typically found in the chemical shifts range comprised between 151 and 155 ppm,

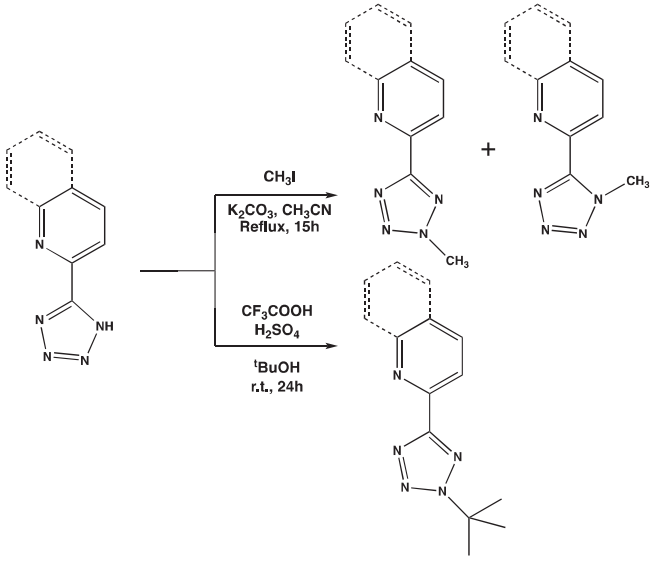

Fig. 2. Functionalization of tetrazole ligands PTZ-H and QTZ-H.

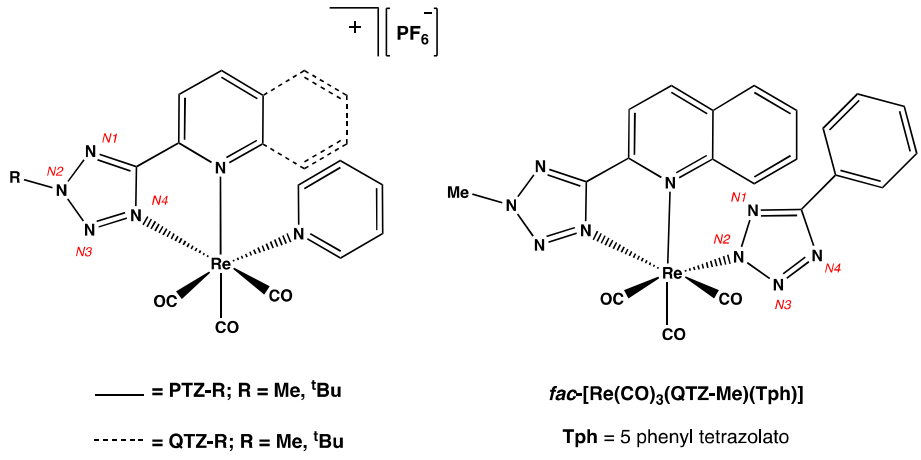

—— = PTZ-R; R = Me, ^{t}Bu

------ = QTZ-R; R = Me, ^{t}Bu

***fac*-[Re(CO)$_3$(QTZ-Me)(Tph)]**

Tph = 5 phenyl tetrazolato

Fig. 1. Re(I) triscarbonyl complexes presented in this work and atom numbering of the tetrazole ring.

the isolation of **PTZ-Me** and **QTZ-Me** as the N-2 alkylated regioisomers was confirmed by the significant downfield shifting of the corresponding C_t signals to chemical shift values ranging from 164 −168 ppm [10].

The reaction of $Re(CO)_5Br$ with a slight molar excess (1:1.2) of the N-2 substituted tetrazole **PTZ-R** or **QTZ-R** in toluene at the reflux temperature led, in all cases, to the isolation of one single and neutrally charged product (Scheme 1), as suggested by electrospray ionization mass spectrometry (ESI-MS) experiments. For all of the new Re(I) complexes, the facial (*fac*) configuration of the three CO ligands was suggested by their displaying solid state infrared (IR) spectra (see Experimental and ESI†, Table S1) consisting of one sharp band at *ca.* 2031 cm^{-1}, that is assigned to the totally symmetric in- phase stretching A′(1), followed by two broader bands at *ca.* 1906 and 1930 cm^{-1}, which results from the of the totally symmetric out-of-phase stretching A′(2) and the asymmetric stretching A″ [11].

The presence of **PTZ-R** or **QTZ-R** ligands in the structure of the Re(I) complexes and, in particular, their adopting the desired chelate coordination to the Re(I) center, was suggested by the comparison of the ^1H NMR spectra of ***fac*-[Re(CO)$_3$(PTZ-R)(Br)]** and ***fac*-[Re(CO)$_3$(QTZ-R)(Br)]** with those of the free ligands **PTZ-R** and **QTZ-R**, respectively. As for instance, in the exemplar case described in Fig. 3, it was possible to observe that in complex ***fac*-[Re(CO)$_3$(QTZ-^{t}Bu)(Br)]**, the bis chelate coordination of **QTZ-^{t}Bu** - while forcing the ligand to a strictly coplanar arrangement - led to the appearance of a different and much better resolved pattern of aromatic signals than the one recorded from **QTZ-^{t}Bu** as a "free" ligand, in which the mutual rotation of the tetrazole and the quinolyl ring is not prevented.

In the successive stage, the obtained complexes ***fac*-[Re(CO)$_3$(PTZ-R)(Br)]** and ***fac*-[Re(CO)$_3$(QTZ-R)(Br)]** were used as starting materials for reactions aimed at the replacement of the coordinated bromide ion either with a neutrally charged ligand such as pyridine (**pyr**), or with the phenyl tetrazolato anion (**Tph**)$^-$. As the preliminary step, both procedures involved the Ag(I)-assisted substitution of the bromide ion of the ***fac*-[Re(CO)$_3$(PTZ-R)(Br)]** and ***fac*-[Re(CO)$_3$(QTZ-R)(Br)]** precursor complexes with an acetonitrile solvent molecule. The resulting cationic intermediates ***fac*-[Re(CO)$_3$(PTZ-R)(NCCH$_3$)] [PF$_6$]** and ***fac*-[Re(CO)$_3$(QTZ-R)(NCCH$_3$)] [PF$_6$]** were successively treated with an excess of pyridine (**pyr**) in $CHCl_3$, leading to the formation the target cationic complexes ***fac*-[Re(CO)$_3$(PTZ-R)(pyr)] [PF$_6$]** and ***fac*-[Re(CO)$_3$(QTZ-R)(pyr)] [PF$_6$]**, respectively. Along with ESI-MS, these reactions were monitored by IR spectroscopy, enlightening how the transformation of the neutrally charged starting compounds into the cationic products was witnessed by the expected shift to higher wavenumbers of the CO stretchings, whose number and relative intensities were again congruent with the facial arrangement of the CO ligands. Following a closer inspection of the IR profiles (Fig. 4 and Table S1 ESI†) it was possible to notice that, as sometimes reported for the family of ***fac*-[Re(N^N)(CO)$_3$(L)]** -type complexes [12,13], the cationic species ***fac*-[Re(CO)$_3$(PTZ-R)(NCCH$_3$)] [PF$_6$]**, ***fac*-[Re(CO)$_3$(QTZ-R)(NCCH$_3$)] [PF$_6$]**, ***fac*-[Re(CO)$_3$(PTZ-R)(pyr)] [PF$_6$]** and ***fac*-[Re(CO)$_3$(QTZ-R)(pyr)] [PF$_6$]**, displayed the superimposition of the A′(2) and A″ stretching modes into a single broad band. In addition, from the comparison of the IR profiles of ***fac*-[Re(CO)$_3$(PTZ-R)(pyr)] [PF$_6$]** and ***fac*-[Re(CO)$_3$(QTZ-R)(pyr)] [PF$_6$]** with respect to the cationic intermediates ***fac*-[Re(CO)$_3$(PTZ-R)(NCCH$_3$)] [PF$_6$]** and ***fac*-[Re(CO)$_3$(QTZ-R)(NCCH$_3$)] [PF$_6$]**, it was observed that the substitution of coordinated acetonitrile molecule in favor of pyridine (**pyr**) caused the shift towards lower wavenumbers of the pattern relative to the CO stretchings (*ca.* 2030, 1930 and 1905 cm^{-1}), the occurrence of which effect is most likely to ascribe due to the stronger π-acidity of pyridine with respect to that of acetonitrile (Fig. 4).

As reported in Fig. 5 and ESI† Figs. S1-S14, the successful introduction of the pyridine ligand within the first coordination sphere of the Re (I) center was also confirmed by the appearance of the characteristic pattern of signals in the aromatic region in both the ^1H and ^{13}C NMR spectra of the corresponding ***fac*-[Re(CO)$_3$(PTZ-R)(pyr)] [PF$_6$]** and ***fac*-[Re(CO)$_3$(QTZ-R)(pyr)] [PF$_6$]** type species.

In a different instance, the intermediate species ***fac*-[Re(CO)$_3$(QTZ-Me)(CH$_3$CN)] [PF$_6$]** was treated with a slight excess of the 5-(phenyl) tetrazolato anion, abbreviated as **Tph** (Scheme 2). The ESI-MS, IR and NMR spectroscopic characterization of the resulting product provided results congruent with its occurrence as the neutrally charged and "fully-tetrazole" complex ***fac*-[Re(CO)$_3$(QTZ-Me)(Tph)]**, as witnessed by the shift to lower wavenumbers of the *fac*-type CO stretchings pattern and the concomitant appearance of two distinct tetrazole carbon (Ct) resonances in the chemical shift region comprised between 164 and 168 ppm (see ESI† Table S1, and Fig. S14).

3. X-Ray crystallography

Along the series of the new Re(I)-tetrazole complexes, two cationic species – namely, those suggested as ***fac*-[Re(CO)$_3$(QTZ-Me)(pyr)] [PF$_6$]** and ***fac*-[Re(CO)$_3$(PTZ-Me)(pyr)] [PF$_6$]** – afforded crystals suitable for X-ray diffraction. For both complexes, the analysis of their molecular structure (Fig. 6 and Table 1, ESI† Table S2) provided results congruent with the occurrence of the expected octahedral complexes in which the coordination environment of Re(I) ion consisted of three CO ligands arranged in a facial (*fac*) geometry, the pyridyl (**PTZ-Me**) or quinolyl tetrazole (**QTZ-Me**) ligands exerting a bis-chelate coordination, and was completed by pyridine as the "third" monodentate ligand. The two complexes show very similar geometries and bonding parameters. The Re-N distances are in the expected range for Re-N(sp^2) interactions [9,12,14,20]. Re(1)-N(1) distances (2.132(8) and 2.029(6) Å for ***fac*-[Re(CO)$_3$(QTZ-Me)(pyr)] [PF$_6$]** and ***fac*-[Re(CO)$_3$(PTZ-Me)(pyr)] [PF$_6$]**, respectively) involving the five-member tetrazolato ring, are slightly shorter than Re(1)-N(5) (2.276(7) and 2.245(7) Å), involving a condensed six member ring. The Re(1)-N(6) interactions (2.201(7) and 2.210(4) Å) are in the middle, in view of the monodentate nature of the pyridine ring.

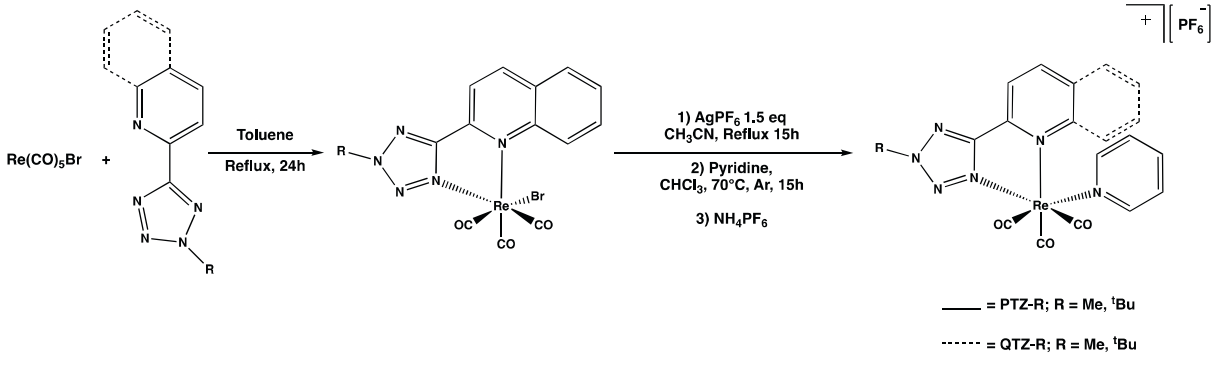

Scheme 1. Synthetic procedure used for the preparation of *fac*-[Re(CO)$_3$(N^N)(pyr)]$^+$ -type complexes.

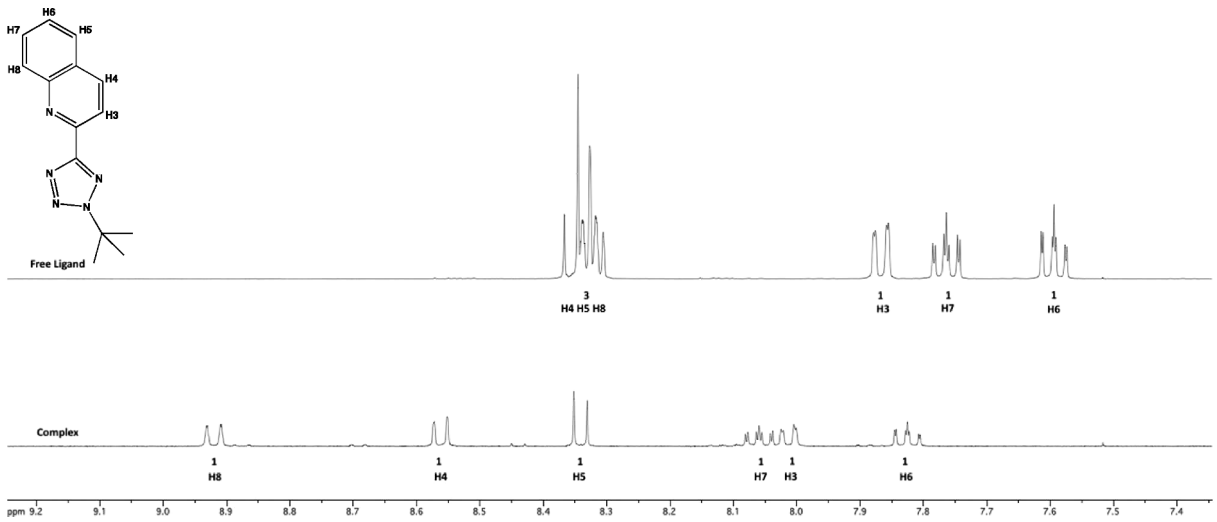

Fig. 3. ^{1}H NMR (aromatic region from 9 to 7.5 ppm) of (**QTZ-^{t}Bu**) (top) and ***fac*-[Re(CO)$_3$(QTZ-^{t}Bu)(Br)]** (bottom) 400 MHz, $CDCl_3$;. "1″ and "3" are referred to the integral value of the resonance above.

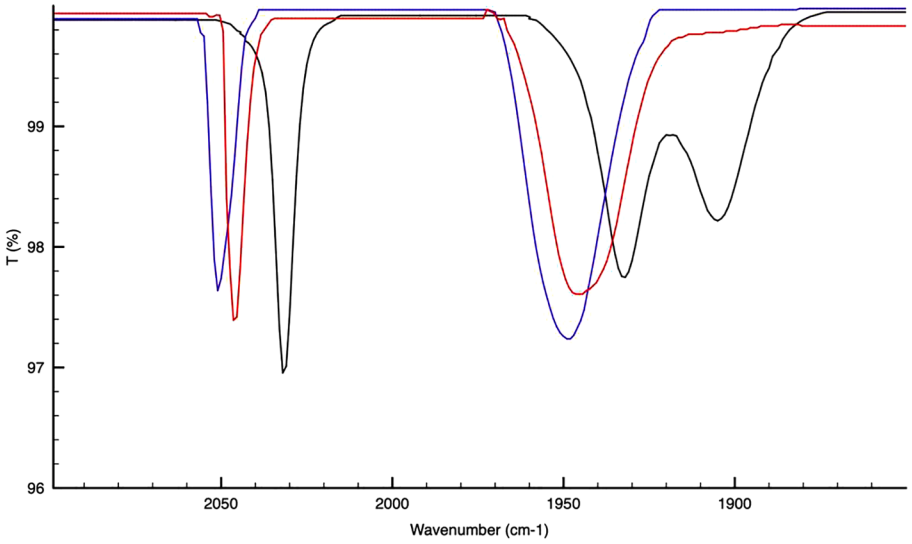

Fig. 4. IR spectra of ***fac*-[Re(CO)$_3$(PTZ-^{t}Bu)(Br)]** (black trace), ***fac*-[Re(CO)$_3$(PTZ-^{t}Bu)(CH$_3$CN)] [PF$_6$]** (blue trace) and ***fac*-[Re(CO)$_3$(PTZ-^{t}Bu)(pyr)] [PF$_6$]** (red trace), FTIR-ATR. (For interpretation of the references to colour in this figure legend, the reader is referred to the web version of this article.)

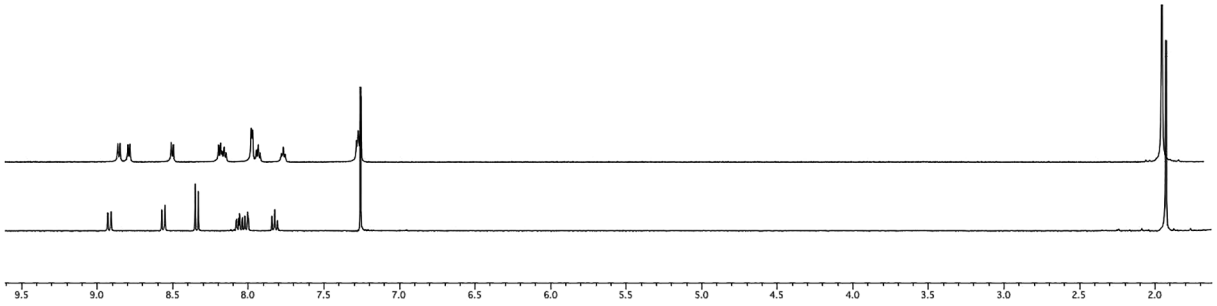

Fig. 5. ^{1}H NMR spectra of ***fac*-[Re(CO)$_3$(QTZ-^{t}Bu)(Br)] [PF$_6$]** (bottom) and ***fac*-[Re(CO)$_3$(QTZ-^{t}Bu)(pyr)] [PF$_6$]** (top), 400 MHz, $CDCl_3$.

4. Photophysical properties

The relevant photophysical data of the target cationic and neutrally charged Re(I) complexes described herein are summarized in Table 2.

As commonly observed for octahedral d^6 metal complexes [1], the absorption profiles of the Re(I) complexes – which were obtained from the corresponding dilute (10^{-5}M) dichloromethane solutions - displayed the UV region dominated by intense ligand-centered (LC) transitions (250–270 nm), followed by metal-to-ligand charge transfer (MLCT) processes (300–410 nm) tailing off in the visible region (See Table 2,

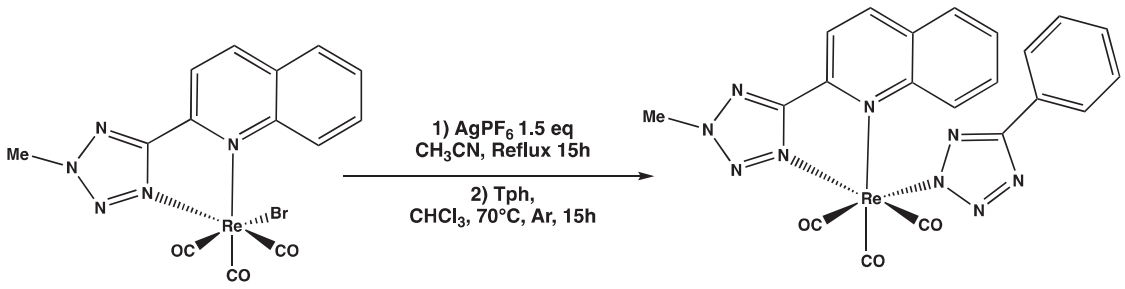

Scheme 2. Synthetic procedure used for the preparation of ***fac*-[Re(CO)$_3$(QTZ-Me)(Tph)]**.

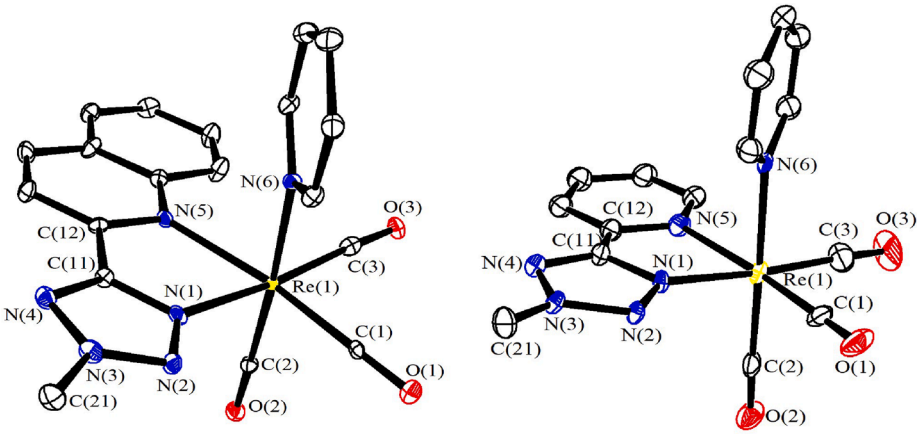

Fig. 6. (left) Molecular structure of ***fac*-[Re(CO)$_3$(QTZ-Me)(pyr)] [PF$_6$]** with key atoms labeled. Displacement ellipsoids are presented at the 30% probability level, $[PF_6]^-$ and H-atoms are omitted for clarity; (right) Molecular structure of ***fac*-[Re(CO)$_3$(PTZ-Me)(pyr)] [PF$_6$]** with key atoms labeled. Displacement ellipsoids are presented at the 30% probability level, $[PF_6]^-$ and H-atoms are omitted for clarity.

Table 1
Selected bond lengths (Å) and angles (°) for ***fac*-[Re(CO)$_3$(QTZ-Me)(pyr)] [PF$_6$]** and complex ***fac*-[Re(CO)$_3$(PTZ-Me)(pyr)] [PF$_6$]**

Selected bond	*fac*-[Re(CO)$_3$(QTZ-Me)(pyr)] [PF$_6$]	*fac*-[Re(CO)$_3$(PTZ-Me)(pyr)] [PF$_6$]
Re(1)-C(1)	1.923(9)	1.927(9)
Re(1)-C(2)	1.907(9)	1.939(10)
Re(1)-C(3)	1.928(10)	1.928(11)
Re(1)-N(1)	2.132(8)	2.029(6)
Re(1)-N(5)	2.276(7)	2.245(7)
Re(1)-N(6)	2.201(7)	2.210(4)
C(1)-O(1)	1.149(11)	1.127(11)
C(2)-O(2)	1.164(11)	1.132(11)
C(3)-O(3)	1.147(11)	1.144(12)
N(1)-N(2)	1.315(11)	1.4200*
N(2)-N(3)	1.309(11)	1.4200*
N(3)-N(4)	1.338(11)	1.4200*
N(1)-C(11)	1.343(12)	1.4200*
N(4)-C(11)	1.325(12)	1.4200*
C(11)-C(12)	1.472(12)	1.281(10)
C(12)-N(5)	1.343(12)	1.3900*
N(3)-C(21)	1.457(12)	1.366(15)
Re(1)-C(1)-O(1)	177.9(7)	178.5(9)
Re(1)-C(2)-O(2)	179.0(8)	177.5(8)
Re(1)-C(3)-O(3)	176.6(8)	178.3(11)
C(1)-Re(1)-N(5)	169.9(3)	169.5(4)
C(2)-Re(1)-N(6)	175.9(3)	179.0(3)
C(3)-Re(1)-N(1)	173.4(3)	173.4(5)
N(1)-Re(1)-N(5)	74.1(3)	72.8(4)
Sum angles at N_4C	540.0(15)	540.0*

* The PTZ-Me ligand of ***fac*-[Re(CO)$_3$(PTZ-Me)(pyr)] [PF$_6$]** is disordered and the atoms of the N_4C ring have been constrained to fit a regular pentagon.

Fig. 7 right and ESI† Figs. S15-S34). Upon excitation of the corresponding MLCT features (λ = 370 nm), the cationic ***fac*-[Re(CO)$_3$(PTZ-R)(pyr)]$^+$** and ***fac*-[Re(CO)$_3$(QTZ-R)(pyr)]$^+$** type species and the neutral complex ***fac*-[Re(CO)$_3$(QTZ-Me)(Tph)]** displayed bright luminescence that, in line with the behavior typical of the family of *fac*-Re(I) triscarbonyl diimine complexes, was represented by broad and structureless emission profiles centered between *ca.* 510 nm and 630 nm (see Fig. 7, right). In particular, if the emissions originating from the **PTZ-R**- based complexes ***fac*-[Re(CO)$_3$(PTZ-R)(pyr)]$^+$** were found to span from λ_{max} = 514 nm to λ_{max} = 578 nm, those observed from the series of **QTZ-R** -based cationic derivatives ***fac*-[Re(CO)$_3$(QTZ-R)(pyr)]$^+$** were quite expectedly found to peak at lower energy, as in the cases of for ***fac*-[Re(CO)$_3$(QTZ-Me)(pyr)]$^+$** and ***fac*-[Re(CO)$_3$(QTZ-^{t}Bu)(pyr)]$^+$**, whose emissions being both centred at 604 nm. The further red shift of the emission maxima (λ_{max} = 632 nm) was observed for the neutrally charged "fully tetrazole" complex ***fac*-[Re(CO)$_3$(QTZ-Me)(Tph)]**. However, in all cases, the emission can be confidently described as phosphorescence originating from charge transfer states of triplet multiplicity, ^{3}CT, in a manner analogous to what we have reported previously for neutral and ionic Re(I) tetrazolato complexes [8,9,12,13]. In fact, the excited state lifetime (τ) and quantum yield (Φ) are sensitive to the presence of dissolved dioxygen (Table 2). Further in support of the ^{3}MLCT nature of the emissive excited states was the significant rigidochromic blue shift of the emission that was observed on passing from 298 K to 77 K [15], highlighting an effect that can be ascribed to the ensuing reduction, or almost complete removal, of vibrational and collisional quenching phenomena (Table 2 and ESI† Figs. S15-S34). It is worth noting that under all the different the experimental conditions in which the measurement were carried out (Table 2), the ***fac*-[Re(CO)$_3$(QTZ-R)(L)]$^{0/+}$** type complexes displayed photoluminescence performances superior to those displayed by the parent ***fac*-[Re(CO)$_3$(PTZ-R)(pyr)]$^+$** derivatives, in terms both of higher quantum yields (Φ_{Ar}) and longer emission lifetimes (τ). This

Table 2
Relevant Absorption and Emission data of all the target Re(I) complexes described in this work.

	Absorption	Emission 298 K					Emission 77 K	
Complex CH_2Cl_2 as solvent	λ_{abs} (nm) ($10^{-4}\varepsilon$) ($M^{-1}cm^{-1}$)	λ_{em} (nm)	τ_{air} (ns)[a]	τ_{Ar} (ns)[a]	φ_{air} (%)[b]	φ_{Ar} (%)[b]	λ_{em} (nm)[c]	τ (μs)[c]
***fac*-[Re(CO)$_3$(PTZ-Me)(pyr)]$^+$**	271 (4.82), 362 (0.93)	578	154	494	2.1	7.6	518	6.00
***fac*-[Re(CO)$_3$(PTZ-^{t}Bu)(pyr)]$^+$**	262 (5.41), 337 (1.34)	514	465	2059	2.4	6.4	482	4.06
***fac*-[Re(CO)$_3$(QTZ-Me)(pyr)]$^+$**	256 (7.96), 328 (1.38), 373 (0.92)	604	1025	3226	3.0	18.0	532, 566	11.90
***fac*-[Re(CO)$_3$(QTZ-^{t}Bu)(pyr)]$^+$**	256 (7.49), 328 (1.32), 373 (0.88)	604	876	4040	3.0	19.0	538, 568	9.80
***fac*-[Re(CO)$_3$(QTZ-Me)(Tph)]**	253 (9.68), 324 (1.43), 368 (0.90)	632	407	721	1.5	9.0	536, 574	10.50

[a] : "Air" means air equilibrated solutions, "Ar" means deoxygenated solutions under argon atmosphere;
[b] : $[Ru(bpy)_3]Cl_2/H_2O$ was used as reference for quantum yield determinations ($\Phi_r = 0.028$) [37];
[c] : in frozen CH_2Cl_2.

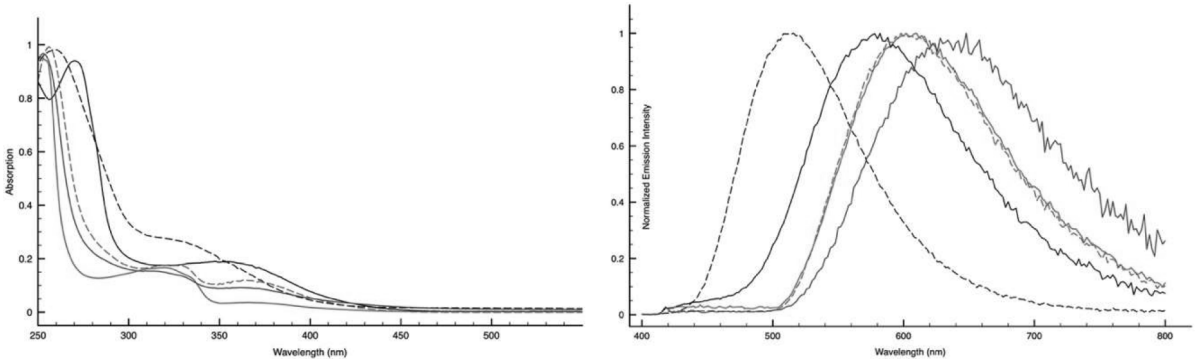

Fig. 7. Normalized absorption profiles (l) and emission profiles (r) of ***fac*-[Re(CO)$_3$(PTZ-Me)(pyr)]$^+$** (black solid line), ***fac*-[Re(CO)$_3$(PTZ-^{t}Bu)(pyr)]$^+$** (black dotted line), ***fac*-[Re(CO)$_3$(QTZ-Me)(pyr)]$^+$** (red solid line), ***fac*-[Re(CO)$_3$(QTZ-^{t}Bu)(pyr)]$^+$** (red dotted line) and ***fac*-[Re(CO)$_3$(QTZ-Me)(Tph)]** (blue solid line), 298 K, CH_2Cl_2. (For interpretation of the references to colour in this figure legend, the reader is referred to the web version of this article.)

trend did become even more evident on passing from air equilibrated to O_2-free solutions, and was quite unexpected in consideration of the energy gap law, since the emission maxima of all the QTZ-R based complexes did peak at significantly lower energies than what observed for the PTZ-R analogous species. Whereas the more extended π-conjugation across the QTZ backbone reasonably accounts for the red shifted emission of the QTZ-R based complexes, their displaying higher quantum yields and longer emission lifetimes might be explained by assuming a likely higher rigidity of the ***fac*-[Re(CO)$_3$(diim)(pyr)]$^+$** structure that is possibly brought by the benzofused **QTZ** scaffold with respect to what happens in the presence of the **PTZ**-based diimine ligand.

5. Interaction with BSA – Bovine serum albumin

Within the general framework of our extensive studies concerning the use of Re(I)-tetrazolato complexes in life science, [8,16–22], we have recently reported the very first examples of Re(I)-based luminescent markers for proteins purified by SDS-PAGE (Sodium Dodecyl Sulphate - PolyAcrylamide Gel Electrophoresis) [9]. In the first stage of those studies, the new Re(I) complexes - which were designed with the general formula *fac*-[Re(CO)$_3$(diim)(L)]$^{0/-}$, where diim could be either bathophenanthroline (BP) or bathophenanthroline disulfonate (BPS) and L was represented by the 5-(phenyl)tetrazolato anion [Tph$^-$] - were successfully screened with respect the luminescent detection of bovine serum albumin (BSA), which is considered as a model protein due to its structural homology with HSA (human serum albumin). Relying on these premises we have endeavored to preliminarily investigate the occurrence of any possible interaction involving BSA and the new complexes ***fac*-[Re(CO)$_3$(diim)(L)]$^{0/+}$** presented herein, namely the cationic species ***fac*-[Re(CO)$_3$(PTZ-R)(pyr)]$^+$** and ***fac*-[Re(CO)$_3$(QTZ-R)(pyr)]$^+$** (R is -Me or -^{t}Bu) and the neutral complex ***fac*-[Re(CO)$_3$(QTZ-Me)(Tph)]**. To this end, both absorption and emission titration experiments were performed by adding 20 × 5 μL (DMSO as the solvent, $2.1*10^{-3}$ M) to 2 mL of BSA as $1*10^{-5}$ M solution in aqueous PBS buffer-(see ESI† Figs. S35-S49). As reported in the literature, [23] the absorption profile of BSA consists of an intense transition centered at 220 nm followed by a weaker band peaking at 280 nm, which are usually assigned to the secondary structure of the protein and the aromatic residues of amino acids, respectively.

Accordingly, whereas the perturbations of the secondary structure of BSA usually lead to a decrease of the absorbance centred at 220 nm, the alterations localized in the surroundings of aromatic residues of amino acids are associated to changes in the process found at 280 nm. Upon incremental additions of $2.1*10^{-3}$ M solutions of Re(I)-tetrazole based species to 2 mL of a 10^{-5}M BSA solution, the resulting absorption profiles presented an ever-growing process at 220 nm, while at higher wavelengths (250–300 nm), overlapped processes from both BSA and Re (I) quenchers were observed, (Fig. 8, left for ***fac*-[Re(CO)$_3$(PTZ-^{t}Bu)(pyr)]$^+$**).

The intrinsic fluorescence of BSA is often referred to the presence of two tryptophan residues, whose accessibility is strictly correlated to the intensity of such emission, as well as the polarity of the solvent used [24]. The occurrence of changes in emission intensity of BSA upon the addition of successive aliquots of a quencher (*i.e.* Re(I) complexes) might be indicative for alteration of the environment that surrounds the protein, suggesting therefore the occurrence of binding interactions between BSA and the quencher. For all the Re(I) complexes presented herein, a decrease in the emission intensity of BSA was always observed as a result of the increased concentration of quencher (0–10^{-4}M). Instead, only in the case of the cationic complex ***fac*-[Re(CO)$_3$(PTZ-^{t}Bu)(pyr)]$^+$** (Fig. 8, right) and the neutrally charged species ***fac*-[Re(CO)$_3$(QTZ-Me)(Tph)]** (Fig. 9, left) an appreciable increase of the Re(I)-based emission intensity was observed.

To get more insights about the quenching mechanism that occurs between BSA and our Re(I) – based quenchers, Stern-Volmer analyses were carried out (Fig. 9 right for ***fac*-[Re(CO)$_3$(QTZ-Me)(Tph)]**, ESI Figs. S35-49 for all the other reported species). In all cases, experimental

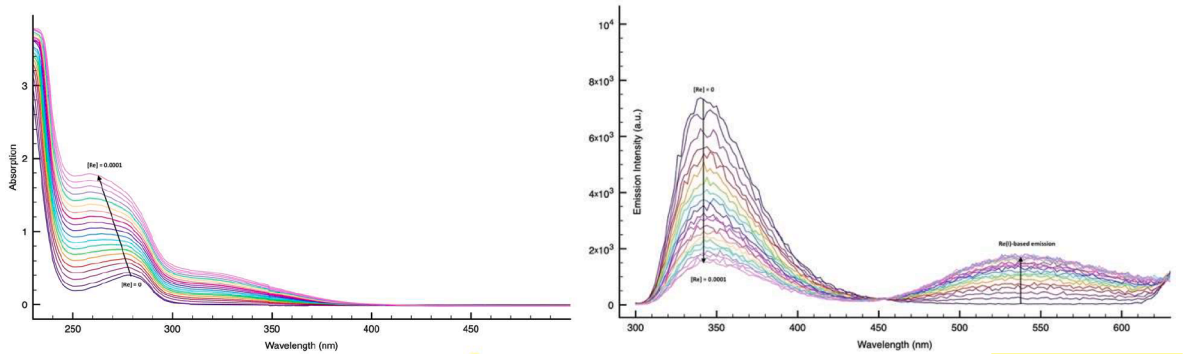

Fig. 8. (l) Absorption Titration of BSA 10^{-5} M/PBS buffer vs ***fac*-[Re(CO)$_3$(PTZ-^{t}Bu)(pyr)]$^+$**, 20x5μL 2.1*10^{-3}M, PBS/DMSO 95:5, 298 K. (r) Emission Titration of BSA 10^{-5} M/PBS buffer vs ***fac*-[Re(CO)$_3$(PTZ-^{t}Bu)(pyr)]$^+$**, 20x5μL 2.1*10^{-3}M, PBS/DMSO 95:5, 298 K. λ_{emi} = 538 nm. λ_{emi} BSA = 346 nm. λ_{exc} = 280 nm.

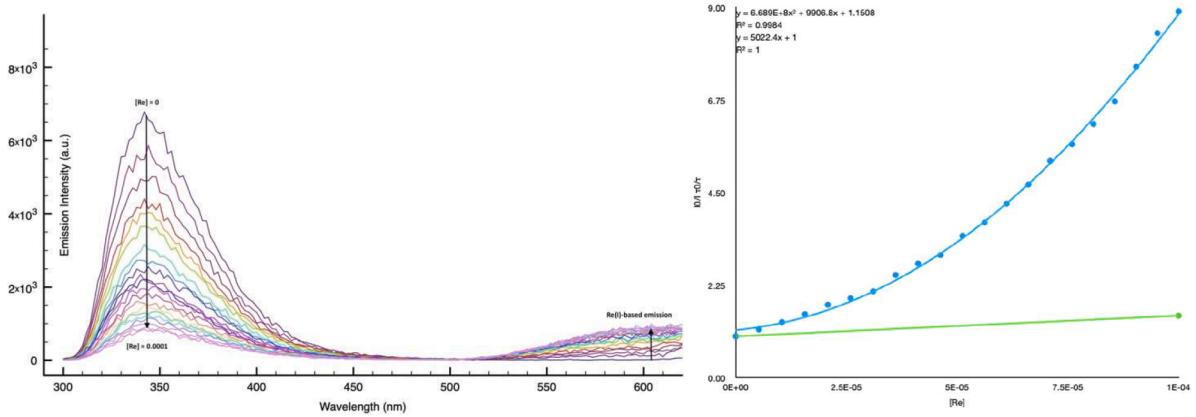

Fig. 9. (l) Emission Titration of BSA 10^{-5} M/PBS buffer vs ***fac*-[Re(CO)$_3$(QTZ-Me)(Tph)]**, 20 × 5 μL 2.1*10^{-3}M, PBS/DMSO 95:5, 298 K. λ_{emi} = 614 nm. λ_{emi} BSA = 346 nm. λ_{exc} = 280 nm; (r) Stern Volmer plot.

results exhibited a non-linear behavior of the I_0/I vs [Q] plot (I_0 and I are the emission intensities of BSA with and without quencher, respectively; [Q] is the concentration of the Re(I)-quencher considered), while the decay time of BSA decreased with increasing concentration of quencher (Table 3). Usually upward curvature of Stern–Volmer plot may be due to (i) static as well as dynamic quenching mechanisms that occurs simultaneously and/or (ii) high extent of quenching at higher concentration region of quencher [25–27]. Thus, a modified Stern-Volmer equation [28] which accounts for the positive curvature observed was used ($F_0/F = (1 + K_D[Q])(1 + K_S[Q])$). Attempts to obtain K_D and K_S values (dynamic and static quenching constants, respectively) using the latter relation were unsuccessful because the resulting quadratic equations were in all cases unsolvable ($\Delta < 0$) [29]. This may be due to the minor contribution of dynamic quenching in the overall process, that was found to range from 10^2 to 10^3 M^{-1} from lifetime data (K_D, Table 3). Moreover, as the resulting bimolecular quenching constants (k_q, Table 3) are higher than the maximum scatter collision-quenching constant of diverse kinds of quenchers for biopolymers fluorescence (2*10^{10} $M^{-1}s^{-1}$), [30,31], the static quenching mechanism seems to be prevalent in the interaction between BSA and the presented Re(I) complexes. On these basis, the affinity (binding constant, k_b) and the number of binding sites (n) of BSA towards our Re(I) complexes were determined according to the Scatchard equation [32–34]. The obtained values (Table 3, ESI Figs. S35–S49) denote an efficient interaction between our Re(I) complexes – in particular, the ones containing the QTZ-based diimine ligands - and BSA, as the optimum range for K_b to be indicative for an efficient process is considered to be 10^4–10^6 L mol^{-1} [35].

6. Conclusions

N-alkylated tetrazoles such as those based of the 2-pyridyl (PTZ) and 2-quynolyl molecular scaffolds, can actually play the role of diimine "diim" ligands for triscarbonyl Re(I) complexes with general formula ***fac*-[Re(CO)$_3$(diim)(L)]$^{0/+}$**. In particular, the analysis of the photophysical behaviour of the new Re (I) complexes, both in the form of cationic species complexes ***fac*-[Re(CO)$_3$(PTZ-R)(pyr)]$^+$**, ***fac*-[Re(CO)$_3$(QTZ-R)(pyr)]$^+$**, where pyr is pyridine, and of the neutrally

Table 3
BSA-Re(I) binding experiments data, 298 K.

Complex PBS/DMSO 95:5, 298 K	λ_{em} (nm)	$\tau^a_{0\ BSA}$ (ns)	τ^a_{BSA} (ns)	τ_0/τ^a_{BSA}	K^b_D (M^{-1})	K^b_q($M^{-1}s^{-1}$)	K^c_b (M^{-1})	n^c
***fac*-[Re(CO)$_3$(PTZ-Me)(pyr)]$^+$**	586	6.7	6.1	1.1	9.8*10^2	1.46*10^{11}	8.8*10^5	1.3
***fac*-[Re(CO)$_3$(PTZ-^{t}Bu)(pyr)]$^+$**	538	6.7	6.2	1.1	8.4*10^2	1.25*10^{11}	1.6*10^5	1.2
***fac*-[Re(CO)$_3$(QTZ-Me)(pyr)]$^+$**	580	6.7	5.1	1.3	3.3*10^3	4.92*10^{11}	2.8*10^6	1.0
***fac*-[Re(CO)$_3$(QTZ-Me)(Tph)]**	614	6.7	4.5	1.5	5.0*10^3	1.49*10^{11}	1.5*10^6	1.3
***fac*-[Re(CO)$_3$(QTZ-^{t}Bu)(pyr)]$^+$**	604	6.7	4.5	1.5	4.8*10^3	7.10*10^{11}	6.8*10^6	1.5

[a]: ±8%, ±16%.[b]: $\tau_0/\tau = 1 + K_D[Q]$. [c]: Derived from Log (I_0-I/I) = Log K + n Log[Q].

charged "fully tetrazole" derivative ***fac*-[Re(CO)$_3$(QTZ-Me)(Tph)]** displayed results in excellent agreement with those usually described for the family of *fac*-Re(I) triscarbonyl diimines. Among the new Re(I) complexes, in particular, unexpectedly efficient emissive performances were exhibited by the whole series of the ***fac*-[Re(CO)$_3$(QTZ-R)(L)]$^{0/+}$** type complexes, enlightening an effect that we have preliminary ascribed to the likely more rigid environment that is brought by the QTZ-based diimine ligands in the corresponding complexes. Another suggestion for the influence played by the **QTZ-R** scaffolds in determining the extent of the various properties of the Re(I) complexes was provided by the results obtained from the preliminary studies about the interaction of the new Re(I) complexes with Bovine Serum Albumin (BSA), as the K_b values for ***fac*-[Re(CO)$_3$(QTZ-R)(L)]$^{0/+}$** type complexes were found to be higher than those relative to ***fac*-[Re(CO)$_3$(PTZ-R)(pyr)]$^+$** series. It is also worth noting that in the cases of ***fac*-[Re(CO)$_3$(PTZ-^{t}Bu)(pyr)]$^+$** and ***fac*-[Re(CO)$_3$(QTZ-Me)(Tph)]**, beyond to the BSA quenching, an appreciable Re(I)-based emission was still observed. Taken together, these preliminary results pave the way for the further development of our Re(I) tetrazole complexes by investigating their interaction toward a wider range of protein targets and by exploring their possible use as luminescent markers for proteins.

7. Experimental section

General considerations All the reagents and solvents were obtained commercially (Sigma Aldrich/Merck, Alfa Aesar, Strem Chemicals) and used as received without any further purification, unless otherwise specified. When required, the reactions were carried out under an argon atmosphere following Schlenk protocols and the purification of the Re(I) complexes was performed via column chromatography with the use of SiO_2 as the stationary phase. ESI-mass spectra were recorded using a Waters ZQ-4000 instrument (ESI-MS, acetonitrile as the solvent). Nuclear magnetic resonance spectra (consisting of ^{1}H and ^{13}C) were always recorded using a Varian Mercury Plus 400 (^{1}H, 399.9; ^{13}C, 101.0 MHz). ^{1}H and ^{13}C chemical shifts were referenced to residual solvent resonances. Infrared Spectra (IR) were acquired with a Perkin Elmer Spectrum One FTIR instrument using the ATR (attenuated total reflectance) module.

Photophysics Absorption spectra were recorded at room temperature using a Perkin Elmer Lambda 35 UV/vis spectrometer. Uncorrected steady-state emission and excitation spectra were recorded on an Edinburgh FLSP920 spectrometer equipped with a 450 W xenon arc lamp, double excitation and single emission monochromators, and a Peltier-cooled Hamamatsu R928P photomultiplier tube (185–850 nm). Emission and excitation spectra were acquired with a cut-off filter (395 nm) and corrected for source intensity (lamp and grating) and emission spectral response (detector and grating) by a calibration curve supplied with the instrument. The wavelengths for the emission and excitation spectra were determined using the absorption maxima of the MLCT transition bands (emission spectra) and at the maxima of the emission bands (excitation spectra). Quantum yields (Φ) were determined using the optically dilute method by Crosby and Demas [36] at excitation wavelength obtained from absorption spectra on a wavelength scale [nm] and compared to the reference emitter by the following equation [37]:

$$\phi_s = \phi_r \left[\frac{A_r(\lambda_r)}{A_s(\lambda_s)}\right]\left[\frac{I_r(\lambda_r)}{I_s(\lambda_s)}\right]\left[\frac{n_s^2}{n_r^2}\right]\left[\frac{D_s}{D_r}\right]$$

where A is the absorbance at the excitation wavelength (λ), I is the intensity of the excitation light at the excitation wavelength (λ), n is the refractive index of the solvent, D is the integrated intensity of the luminescence, and Φ is the quantum yield. The subscripts r and s refer to the reference and the sample, respectively. A stock solution with an absorbance > 0.1 was prepared, then a 10 times diluted solution was obtained, resulting in absorbance of about 0.07/0.08 depending on the sample considered. The Lambert-Beer law was assumed to remain linear at the concentration of the solutions. The degassed measurements were obtained after the solutions were bubbled for 10 min under Ar atmosphere, using a septa-sealed quartz cell. Air-equilibrated $[Ru(bpy)_3]Cl_2/H_2O$ solution ($\Phi = 0.028$) [38] was used as reference. The quantum yield determinations were performed at identical excitation wavelengths for the sample and the reference, therefore deleting the $I(\lambda r)/I(\lambda s)$ term in the equation. Emission lifetimes (τ) were determined with the single photon counting technique (TCSPC) with the same Edinburgh FLSP920 spectrometer using pulsed picosecond LED (EPLED 360, FWHM < 800 ps) as the excitation source, with repetition rates between 1 kHz and 1 MHz, and the above-mentioned R928P PMT as detector. The goodness of fit was assessed by minimizing the reduced $\chi 2$ function and by visual inspection of the weighted residuals. To record the 77 K luminescence spectra, the samples were put in quartz tubes (2 mm diameter) and inserted in a special quartz Dewar filled with liquid nitrogen. The solvent used in the preparation of the solutions for the photophysical investigations was of spectrometric grade. Experimental uncertainties are estimated to be ± 8% for lifetime determinations, ±20% for quantum yields, and ± 2 nm and ± 5 nm for absorption and emission peaks, respectively.

Ligand synthesis Tetrazole derivatives are used as components for explosive mixtures [10]. In this lab, the reactions described here were only run on a few grams scale and no problems were encountered. However, *great caution* should be exercised when handling or heating compounds of this type. Following the general method reported by Koguro and co-workers [39], tetrazole ligands [H-**Tph**], [H-**QTZ**] and [H-**PTZ**] were obtained in almost quantitative yield.

[H-**Tph**] **^{1}H NMR** (DMSOd_6, 400 MHz) δ (ppm) = 8.06–8.03 (m, 2H, H2, H6), 7.62–7.60 (m, 3H, H3, H4, H5); [H-**PTZ**] **^{1}H NMR**, (DMSO-d_6, 400 MHz) δ (ppm): 8.79–8.77 (m, 1H, H6), 8.22–8.20 (m, 1H, H3), 8.08–8.04 (m, 1H, H4), 7.63–7.60 (m, 1H, H5); [H-**QTZ**] **^{1}H NMR**, (DMSO-d_6, 400 MHz) δ (ppm) = 8.65 (d, 1H, $J_{H\text{-}H}$ = 8.79 Hz, H4), 8.31 (d, 1H, $J_{H\text{-}H}$ = 8.40 Hz, H5), 8.17 (d, 1H, $J_{H\text{-}H}$ = 8.40 Hz, H8), 8.12 (d, 1H, $J_{H\text{-}H}$ = 7.99 Hz, H3), 7.90 (t, 1H, H7), 7.74 (t, 1H, H6).

Ligand Functionalization The ligands **PTZ-Me** (N-3), **QTZ-Me** (N-3) and **PTZ-^{t}Bu**, **QTZ-^{t}Bu** were obtained according to previously reported literature procedures [40].

PTZ-Me (N-3) **^{1}H NMR**, ($CDCl_3$, 400 MHz) δ (ppm): 8.67–8.65 (m,1H, H6), 8.13–8.10 (m, 1H, H3), 7.77–7.73 (m, 1H, H4), 7.30–7.26 (m, 1H, H5), 4.34 (s, 3H, CH_3). **^{13}C NMR**, ($CDCl_3$, 100 MHz) δ (ppm): 164.78 (C_t), 150.18 (C_{ipso}), 146.60 (C6), 137.00 (C4), 124.73 (C3), 122.20 (C5), 39.59 (CH_3) [40].

QTZ-Me (N-3) **^{1}H NMR**, ($CDCl_3$, 400 MHz) δ (ppm): 8.38–8.36 (m, 3H, H8, H5, H4), 7.91–7.88 (m, 1H, H7), 7.82–7.76 (m, 1H, H3), 7.65–7.61 (m, 1H, H6), 4.52 (s, 3H, CH_3). **^{13}C NMR**, ($CDCl_3$, 100 MHz) δ (ppm): 164.98 (C_t), 148.01 (C_{ipso}), 146.49 (C10), 137.25 (C4), 130.01 (C8), 129.93 (C5), 128.32 (C6), 127.54 (C7), 127.42 (C9), 119.54 (C3), 39.71 (CH_3) [40].

PTZ-^{t}Bu ^{1}H NMR, ($CDCl_3$, 400 MHz) δ (ppm): 8.81–8.80 (d, 1H, $J_{H\text{-}H}$ = 4.00 Hz, H6), 8.28–8.26 (d, 1H, $J_{H\text{-}H}$ = 7.60 Hz, H3), 7.88–7.84 (m, 1H, H4), 7.40–7.37 (m, 1H, H5), 1.84 (s, 9H, -^{t}Bu). **^{13}C NMR**, ($CDCl_3$, 100 MHz) δ (ppm): 164.1 (C_t), 155.2 (C_{ipso}), 149.4, 137.2, 124.2, 123.7, 73.1 (C-$(CH_3)_3$), 28.3 ($(CH_3)_3$).

QTZ-^{t}Bu ^{1}H NMR, ($CDCl_3$, 400 MHz) δ (ppm): 8.38 – 8.30 (m, 3H, H4, H5, H8), 7.87 (m, 1H, H3), 7.77 (m, 1H, H7), 7.60 (m, 1H, H6), 1.87 (s, 9H, -^{t}Bu). **^{13}C NMR**, ($CDCl_3$, 100 MHz) δ (ppm): 163.5 (C_t), 157.4 (C_{ipso}), 144.2 (C10), 137.3 (C4), 129.8 (C8), 128.3 (C6), 127.1 (C7), 125.3 (C5), 121.0 (C9), 119.5 (C3), 72.9 (C-$(CH_3)_3$), 28.6 ($(CH_3)_3$).

7.1. General procedure for the preparation of *fac*-[Re(CO)$_3$(N^N)-(pyr)]$^+$ -type complexes and *fac*-[Re(CO)$_3$(QTZ-Me)-(Tph)]

The preparation of ***fac*-[Re(CO)$_3$(N^N)-(pyr)]$^+$** -type complexes was accomplished by following a multistep procedure which involved at first the formation of the neutral *fac*-[Re(CO)$_3$(N^N)(Br)] by refluxing Re

$(CO)_5Br$ (1 eq) with the appropriate (N^N) ligand (1.1 eq) in 20 mL of toluene for 24 h. The crude was allowed to cool to room temperature and the addition of Et_2O induced the precipitation of bright yellow to orange solids collected by filtration, air-dried and used for the successive steps without any further purification. In a two neck round bottomed flask protected from light, 1 eq of the desired neutral *fac*-[$Re(CO)_3$(N^N)(Br)] and 1.5 eq. of $AgPF_6$ were combined in 20 mL of CH_3CN and refluxed for 3 hrs. The crude was cooled to room temperature, filtered over a celite pad to remove AgBr and successively combined with pyridine (5 eq.) in $CHCl_3$ (20 mL) .The solutions were heated over reflux (70 °C) under an argon atmosphere for 15 hrs, after which the pale to bright yellow precipitates formed were collected by filtration and washed with Et_2O. In the case of ***fac*-[Re(CO)$_3$(QTZ-Me)(Tph)]**, 1.2 eq. of H-Tph were added to the reaction mixture instead of pyridine after the halide extraction step. The crude was then purified by column chromatography over SiO_2 eluted with a CH_2Cl_2/Acetone 9:1 mixture. Product in F1.

***fac*-[Re(CO)$_3$(PTZ-Me)(Br)] ^{1}H NMR**, ($CDCl_3$, 400 MHz) δ (ppm): 9.11–9.09 (m, 1H, H6), 8.28–8.25 (m, 1H, H3), 8.16–8.11 (m, 1H, H4), 7.65–7.62 (m, 1H, H5), 4.59 (s, 3H, CH_3). **ESI-MS** (*m/z*): $[M + Na]^+$ = 534, $[M + K]^+$ = 550. **IR-ATR** ν (cm^{-1}): 2033 (CO), 1934 (CO), 1907 (CO). Y = 69% (MW = 511 g/mol, 0.35 mmol).

***fac*-[Re(CO)$_3$(PTZ-^{t}Bu)(Br)] ^{1}H NMR**, ($CDCl_3$, 400 MHz) δ (ppm): 9.10–9.08 (m, 1H, H6), 8.30–8.26 (m, 1H, H3), 8.14–8.10 (m, 1H, H4), 7.63–7.59 (m, 1H, H5), 1.88 (s, 9H, -^{t}Bu). **ESI-MS** (*m/z*): $[M + Na]^+$ = 575. **IR-ATR** ν (cm^{-1}): 2032 (CO), 1933 (CO), 1905 (CO). Y = 19% (MW = 552 g/mol; 0.05 mmol).

***fac*-[Re(CO)$_3$(QTZ-Me)(Br)] ^{1}H NMR**, (Acetone-d_6, 400 MHz) δ (ppm): 9.01–8.99 (d, 1H, J_{H-H} = 8.80 Hz, H8), 8.87–8.85 (d, 1H, J_{H-H} = 8.80 Hz, H4), 8.53–8.51 (d, 1H, J_{H-H} = 8.40 Hz, H5), 8.34–8.32 (d, 1H, J_{H-H} = 8.00 Hz, H3), 8.24–8.20 (t, 1H, J_{H-H} = 16.00 Hz, J_{H-H} = 8.40 Hz, J_{H-H} = 7.60 Hz, H7), 8.00–7.96 (t, 1H, J_{H-H} = 15.2 Hz, J_{H-H} = 8.00 Hz, J_{H-H} = 7.20 Hz, H6), 4.83 (s, 3H, CH_3). **ESI-MS** (*m/z*): $[M + Na]^+$ = 584 *m/z*. **IR-ATR** ν (cm^{-1}): 2031 (CO), 1931 (CO), 1910 (CO). Y = 73% (MW = 561 g/mol, 0.51 mmol).

***fac*-[Re(CO)$_3$(QTZ-^{t}Bu)(Br)] ^{1}H NMR**, ($CDCl_3$, 400 MHz) δ (ppm): 8.93–8.91 (d, 1H, J_{H-H} = 8.00 Hz, H8), 8.58–8.56 (d, 1H, J_{H-H} = 8.0 Hz, H4), 8.35–8.33 (d, 1H, J_{H-H} = 8.40 Hz, H5), 8.10–8.01 (m, 2H, H3, H7), 7.90–7.81 (m, 1H, H6), 1.93 (s, 9H, -^{t}Bu). **ESI-MS** (*m/z*): $[M + Na]^+$ = 626, $[M + K]^+$ = 642. **IR-ATR** ν (cm^{-1}): 2031 (CO), 1930 (CO), 1907 (CO). Y = 73% (MW = 553 g/mol, 0.60 mmol). Y = 41% (MW = 603 g/mol, 0.14 mmol).

***fac*-[Re(CO)$_3$(PTZ-Me)-(pyr)] [PF$_6$] ^{1}H NMR**, (Acetone-d_6, 400 MHz) δ (ppm): 9.56–9.54 (m, 1H, PTZ-Me), 8.55–8.52 (m, 3H, pyr), 8.51–8.46 (m, 1H, PTZ-Me), 8.11–8.07 (m, 1H, PTZ-Me), 8.02–7.97 (m, 1H, PTZ-Me), 7.48–7.45 (m, 2H, pyr), 4.75 (s, 3H, CH_3). **IR-ATR** ν (cm^{-1}): 2036.2 (CO), 1913.6 (CO). **ESI-MS** (*m/z*): $[M]^+$ = 511; $[M]^-$ = 145 (PF_6). **^{13}C NMR**, (Acetone-d_6, 100 MHz) δ (ppm): 167.18 (C_t), 155.29 (C_{ipso}), 152.65 (PTZ-Me), 144.56 (pyr), 142.47 (PTZ-Me), 140.16 (pyr), 130.44 (PTZ-Me), 127.07 (PTZ-Me), 124.84 (pyr), 42.03 (CH_3). Y = 75% (MW = 655 g/mol; 0.303 mmol). Anal. Calcd. For $C_{15}H_{12}N_6O_3P_1F_6Re_1$ (655.47) C 27.49, H 1.85, N 12.82. Found: C 24.8, H 1.69, N 10.85.

***fac*-[Re(CO)$_3$(PTZ-^{t}Bu)-(pyr)] [PF$_6$] ^{1}H NMR**, ($CDCl_3$, 400 MHz) δ (ppm): 9.17–9.16 (d, 1H, J_{H-H} = 5.60 Hz, PTZ-^{t}Bu), 8.44–8.42(d, 1H, J_{H-H} = 7.20 Hz, pyr), 8.34–8.30 (m, 1H, PTZ-^{t}Bu), 8.26–8.24 (d, 2H, J_{H-H} = 5.20 Hz, PTZ-^{t}Bu), 7.91–7.81 (m, 2H, pyr), 7.43–7.40 (m, 2H, pyr), 1.92 (s, 9H, -^{t}Bu). **ESI-MS** (*m/z*): $[M]^+$ = 553; $[M]^-$ = 145 (PF_6). **IR-ATR** ν (cm^{-1}): 2045 (CO), 1940 (CO). **^{13}C NMR**, (Acetone-d_6, 100 MHz) δ (ppm): 166.98 (C_t), 155.22 (C_{ipso}), 152.61 (PTZ-^{t}Bu), 144.93 (pyr), 142.37 (PTZ-^{t}Bu), 140.20 (pyr), 130.32 (PTZ-^{t}Bu), 127.06 (PTZ-^{t}Bu), 124.84 (pyr), 69.36 (C^tBu), 40.55 (-^{t}Bu). Y = 19% (MW = 698 g/mol; 0.05 mmol). Anal. Calcd. For $C_{18}H_{18}N_6O_3P_1F_6Re_1$ (697.55) C 30.99, H 2.60, N 12.05. Found: C 29.43, H 2.45, N 11.94.

***fac*-[Re(CO)$_3$(QTZ-Me)-(pyr)] [PF$_6$] ^{1}H NMR**, (CD_3CN, 400 MHz) δ (ppm): 8.95–8.88 (m, 1H, QTZ-Me), 8.49–8.47 (d, 1H, J_{H-H} = 8.0 Hz, QTZ-Me), 8.31–8.27 (m, 2H, QTZ-Me, pyr), 8.17–8.15 (m, 1H, QTZ-Me), 8.03–8.00 (m, 2H, pyr), 7.86–7.80 (m, 2H, pyr), 7.70–7.66 (m, 1H, QTZ-Me), 7.23–7.20 (m, 1H, QTZ-Me), 4.46 (s, 3H, CH_3). **ESI-MS** (*m/z*): $[M]^+$ = 561; $[M]^-$ = 145 (PF_6). **IR-ATR** ν (cm^{-1}): 2045 (CO), 1940 (CO). **^{13}C NMR**, (CD_3CN, 100 MHz) δ (ppm): 166.78 (C_t), 152.53 (C_{ipso}), 147.44 (QTZ-Me), 143.73 (pyr), 139.94 (pyr), 138.34 (QTZ-Me), 134.84 (QTZ-Me), 131.02 (QTZ-Me), 130.81 (QTZ-Me), 130.44 (QTZ-Me), 130.31 (QTZ-Me), 129.40 (QTZ-Me), 128.94 (QTZ-Me), 128.76 (QTZ-Me), 128.18 (QTZ-Me), 126.93 (pyr), 119.99 (QTZ-Me), 42.39 (CH_3). Y = 34% (MW = 705 g/mol; 0.088 mmol). Anal. Calcd. For $C_{19}H_{14}N_6O_3P_1F_6Re_1$ (705.53) C 32.35, H 2.00, N 11.91. Found: C 30.39, H 2.04, N 10.63.

***fac*-[Re(CO)$_3$(QTZ-^{t}Bu)-(pyr)] [PF$_6$] ^{1}H NMR**, ($CDCl_3$, 400 MHz) δ (ppm): 8.87–8.85 (d, 1H, J_{H-H} = 8.80 Hz, QTZ-^{t}Bu), 8.80–8.78 (d, 1H, J_{H-H} = 8.40 Hz, QTZ-^{t}Bu), 8.53–8.51 (d, 1H, J_{H-H} = 8.40 Hz, QTZ-^{t}Bu), 8.20–8.14 (m, 2H, pyr), 8.00–7.98 (d, 2H, J_{H-H} = 5.20 Hz, QTZ-^{t}Bu), 7.96–7.92 (m, 1H, QTZ-^{t}Bu), 7.79–7.76 (t, 1H, J_{H-H} = 15.60 Hz, J_{H-H} = 8.00 Hz, J_{H-H} = 7.60 Hz, pyr), 7.30–7.26 (m, 2H, pyr), 1.96 (s, 9H, -^{t}Bu). **ESI-MS** (*m/z*): $[M]^+$ = 603, $[M]^-$ = 145 (PF_6). **IR-ATR** ν (cm^{-1}): 2030 (CO), 1926 (CO), 1940 (CO). **^{13}C NMR** ($CDCl_3$, 100 MHz) δ (ppm): 167.60 (C_t), 151.73 (C_{ipso}), 147.18 (QTZ-^{t}Bu), 143.42 (pyr), 140.21 (pyr), 134.33 (QTZ-^{t}Bu), 130.83 (QTZ-^{t}Bu), 130.50 (QTZ-^{t}Bu), 130.15 (QTZ-^{t}Bu), 128.55 (QTZ-^{t}Bu), 127.26 (QTZ-^{t}Bu), 121.08 (pyr), 105.01 (QTZ-^{t}Bu), 70.01 (^{t}Bu), 29.63 (^{t}Bu). Y = 12% (MW = 748 g/mol; 0.016 mmol). Anal. Calcd. For $C_{22}H_{20}N_6O_3P_1F_6Re_1$ (747.61) C 35.35, H 2.70, N 11.24. Found: C 36.27, H 2.91, N 11.03.

***fac*-[Re(CO)$_3$(QTZ-Me)(Tph)] ^{1}H NMR**, ($CDCl_3$, 400 MHz) δ (ppm): 8.99–8.97 (d, 1H, J_{H-H} = 8.80 Hz, QTZ-Me), 8.59–8.57 (d, 1H, J_{H-H} = 8.40 Hz, QTZ-Me), 8.33–8.31 (d, 1H, J_{H-H} = 8.40 Hz, QTZ-Me), 8.07–8.03 (m, 1H, QTZ-Me), 8.00–7.98 (m, 1H, QTZ-Me), 7.86–7.84 (m, 2H, Tph), 7.82–7.78 (m,1H, QTZ-Me), 7.31–7.24 (m, 3H, Tph), 4.64 (s, 3H, CH_3). **ESI-MS** (*m/z*): [M + H] = 628 *m/z*. **IR-ATR** ν (cm^{-1}): 2036 (CO), 1932 (CO). **^{13}C NMR**, (Acetone-d_6, 100 MHz) δ (ppm): 197.34 (CO), 194.13 (CO), 193.09 (CO), 168.91 (C_t, QTZ-Me), 162.65 (C_t, Tph), 148.08 (C_{ipso}), 147.57 (C_{ipso}), 133.54 (QTZ-Me), 130.22 (QTZ-Me), 130.17 (QTZ-Me), 129.77 (QTZ-Me), 129.74 (QTZ-Me), 129.56 (Tph), 128.41 (Tph), 128.30 (QTZ-Me), 128.14 (QTZ-Me), 125.81 (Tph), 119.46 (QTZ-Me), 41.69 (CH_3). Y = 48% (MW = 627 g/mol; 0.12 mol). Anal. Calcd. For $C_{21}H_{14}N_9O_3Re_1$ (626.6) C 40.25, H 2.25, N 20.12. Found: C 37.14, H 2.27, N 17.72.

Absorption and Emission Titration Experiments PBS buffer (1 L) was prepared by dissolving Na_2HPO_4 (1.44 g), KH_2PO_4 (0.245 g), NaCl (8 g) and KCl (0.2 g) in 0.8 L of H_2O. After complete mixing, the solution was topped up to volume. Final pH = 7.4. Then, a 100 mL $4.4*10^{-4}$ M BSA (Sigma Aldrich, MW = 66463 g/mol) solution was prepared by dissolving 2.9 g of BSA in 100 mL of PBS buffer. The final concentration of BSA used in the absorption and emission titration was $1*10^{-5}$M (45.45 μL of $4.4*10^{-4}$ M BSA to V_{tot} = 2 mL). The Re(I)-complexes solutions were prepared by dissolving 1.2–1.4 mg of complex in 1 mL of DMSO, resulting in concentrations of $2.1*10^{-3}$ M. 2 mL of the BSA/PBS solution were placed in a quartz cuvette and successive aliquots of Re(I) complexes solutions in DMSO were added with a micropipette (20x5μL). For absorption titration, absorption spectra were collected from 230 to 800 nm after each addition. For emission titration, emission spectra were collected from 300 to 800 nm by monitoring the 346 nm maxima (BSA emission) upon 280 nm excitation.

X-ray crystallography Crystal data and collection details for ***fac*-[Re(PTZ-Me)(CO)$_3$(pyr)] [PF$_6$]·CH$_2$Cl$_2$** and ***fac*-[Re(QTZ-Me)(CO)$_3$(pyr)] [PF$_6$]·CHCl$_3$** are reported in ESI†, Table S2. Data were recorded on a Bruker APEX II diffractometer equipped with a PHOTON2 (***fac*-[Re(QTZ-Me)(CO)$_3$(pyr)] [PF$_6$]·CHCl$_3$**) or CCD (***fac*-[Re(PTZ-Me)(CO)$_3$(pyr)] [PF$_6$]·CH$_2$Cl$_2$**) detector using Mo–Kα radiation. Data were corrected for Lorentz polarization and absorption effects (empirical absorption correction SADABS) [41]. The structures were solved by direct methods and refined by full-matrix least-squares based on all data using F^2 [42]. Hydrogen atoms were fixed at calculated positions and refined by a riding model. All non-hydrogen atoms were refined with

anisotropic displacement parameters. The PTZ-Me ligand and $[PF_6]^-$ anion of ***fac*-[Re(PTZ-Me)(CO)$_3$(pyr)] [PF$_6$]·CH$_2$Cl$_2$** are disordered. They have been split into two positions and refined using one occupancy factor per disordered group. CCDC 2,044,691 and 2,044,692 contains the supplementary crystallographic data for ***fac*-[Re(PTZ-Me)(CO)$_3$(pyr)] [PF$_6$]·CH$_2$Cl$_2$** and ***fac*-[Re(QTZ-Me)(CO)$_3$(pyr)] [PF$_6$]·CHCl$_3$**. These data can be obtained free of charge via http://www.ccdc.cam.ac.uk/conts/retrieving.html, or from the Cambridge Crystallographic Data Centre, 12 Union Road, Cambridge CB2 1EZ, UK; fax: (+44) 1223–336-033; or e-mail: deposit@ccdc.cam.ac.uk.

Declaration of Competing Interest

The authors declare that they have no known competing financial interests or personal relationships that could have appeared to influence the work reported in this paper.

Acknowledgments

The authors wish to thank the Italian Ministry of Education, University and Research (MIUR) for financial support (PRIN project: Towards a Sustainable Chemistry: Design of Innovative Metal-Ligand Systems for Catalysis and Energy Applications). The Overseas (grant for E.B.) and Marco Polo (grant for N.M.) programmes joint by University of Bologna and the Curtin University of Perth are gratefully acknowledged.

Appendix A. Supplementary data

Supplementary data to this article can be found online at https://doi.org/10.1016/j.ica.2020.120244.

References

[1] R. A. Kirgan, B. P. Sullivan and D-P. Rillema, Photochemistry and Photophysics of Coordination Compounds: Rhenium. In: V. Balzani, S. Campagna (eds.) "Photochemistry and Photophysics of Coordination Compounds II", Top. Curr. Chem., 2007, 281, 45-100. DOI:10.1007/128_2007_143.

[2] a) K. Y. Zhang and K. K.-W. Lo, "Chemosensing and Diagnostics", in Coordination and Organometallic Chemistry of Comprehensive Inorganic Chemistry II, ed. V. W.-W. Yam, Elsevier, Amsterdam, 2013, 8, 657–732, and references cited therein. DOI: 10.1016/B978-0-08-097774-4.00804-4.

[3] S. Hostachy, C. Policar, N. Delsuc, Re(I) carbonyl complexes: multimodal platforms for inorganic chemical biology, Coord. Chem. Rev. 351 (2017) 172–188.

[4] K.K.-W. Lo, Luminescent Rhenium(I) and Iridium(III) polypyridine complexes as biological probes, imaging reagents, and photocytotoxic agents, Acc. Chem. Res. 12 (2015) 2985–2995, https://doi.org/10.1016/j.ccr.2017.05.004.

[5] L.C.-C. Lee, K.-K. Leung, K.K.-W. Lo, Recent development of luminescent rhenium (I) tricarbonyl polypyridine complexes as cellular imaging reagents, anticancer drugs, and antibacterial agents, Dalton Trans. 46 (2017) 16357–16380, https://doi.org/10.1039/C7DT03465B.

[6] V. Fernandez-Moreira, F.L. Thorp-Greenwood, M.P. Coogan, Application of d6 transition metal complexes in fluorescence cell imaging, Chem. Commun. 46 (2010) 186–202, https://doi.org/10.1039/B917757D.

[7] F.L. Thorp-Greenwood, M.P. Coogan, L. Mishra, N. Kumari, G. Raic, S. Saripellad, The importance of cellular localisation of probes: synthesis, photophysical properties, DNA interactions and cellular imaging properties of rhenium dppz complexes with known cellular localisation vectors, New J. Chem. 36 (2012) 64–72, https://doi.org/10.1039/C1NJ20662A.

[8] C.A. Bader, R.D. Brooks, Y.S. Ng, A. Sorvina, M.V. Werrett, P.J. Wright, A. G. Anwer, D.A. Brooks, S. Stagni, S. Muzzioli, M. Silberstein, B.W. Skelton, E. M. Goldys, S.E. Plush, T. Shandala, M. Massi, Modulation of the cellular organelle specificity in Re(I) tetrazolato complexes leads to unprecedented phosphorescent labeling of lipid droplets, RSC Adv. 4 (2014) 16345–16351, https://doi.org/10.1039/C4RA00050A.

[9] V. Fiorini, L. Bergamini, N. Monti, S. Zacchini, S.E. Plush, M. Massi, A. Hochkoeppler, A. Stefan, S. Stagni, Luminescent protein staining with Re(I) tetrazolato complexes, Dalton Trans. 47 (2018) 9400–9410, https://doi.org/10.1039/C8DT02052C.

[10] R.N. Butler, Tetrazoles, in: R.C. Storr (Ed.), Comprehensive Heterocyclic Chemistry II, Pergamon Press, Oxford, U.K., 1996, pp. 621–678, and references cited therein.

[11] S. Sato, T. Morimoto, O. Ishitani, Photochemical synthesis of mer-[Re(bpy)(CO)3Cl], Inorg. Chem. 46 (2007) 9051–9053, https://doi.org/10.1021/ic701458h.

[12] M.V. Werrett, D. Chartrand, J.D. Gale, G.S. Hanan, J.G. MacLellan, M. Massi, S. Muzzioli, P. Raiteri, B.W. Skelton, M. Silberstein, S. Stagni, Synthesis, structural, and photophysical investigation of diimine triscarbonyl Re(I) tetrazolato complexes, Inorg. Chem. 50 (2011) 1229–1241, https://doi.org/10.1021/ic1015516.

[13] M.V. Werrett, S. Muzzioli, P.J. Wright, A. Palazzi, P. Raiteri, S. Zacchini, M. Massi, S. Stagni, Proton-induced reversible modulation of the luminescent output of rhenium(I), iridium(III), and ruthenium(II) tetrazolate complexes, Inorg. Chem. 53 (2014) 229–243, https://doi.org/10.1021/ic402187e.

[14] M.V. Werrett, G.S. Huff, S. Muzzioli, V. Fiorini, S. Zacchini, B.W. Skelton, A. Maggiore, J.M. Malicka, M. Cocchi, K.C. Gordon, S. Stagni, M. Massi, Methylated Re(I) tetrazolato complexes: photophysical properties and light emitting devices, Dalton Trans. 44 (2015) 8379–8393, https://doi.org/10.1039/C4DT03228D.

[15] L. Flamigni, A. Barbieri, C. Sabatini, B. Ventura and F. Barigelletti, Photochemistry and Photophysics of Coordination Compounds: Iridium. In: V. Balzani, S. Campagna (eds) "Photochemistry and Photophysics of Coordination Compounds II", Top. Curr. Chem., 2007, 281, 143-203. DOI:10.1007/128_2007_131.

[16] N. Akabar, V. Chaturvedi, G.E. Shillito, B.J. Schwehr, K.C. Gordon, G.S. Huff, J. J. Sutton, B.W. Skelton, A.N. Sobolev, S. Stagni, D.J. Nelson, M. Massi, Photophysical and biological investigation of phenol substituted rhenium tetrazolato complexes, Dalton Trans. 48 (2019) 15613–15624, https://doi.org/10.1039/c9dt02198a.

[17] J.L. Wedding, H.H. Harris, C.A. Bader, S.E. Plush, R. Mak, M. Massi, D.A. Brooks, B. Lai, S. Vogt, M.V. Werrett, P.V. Simpson, B.W. Skelton, S. Stagni, Intracellular distribution and stability of a luminescent rhenium(I) tricarbonyl tetrazolato complex using epifluorescence microscopy in conjunction with X-ray fluorescence imaging, Metallomics 9 (2017) 382–390, https://doi.org/10.1039/c6mt00243a.

[18] C.A. Bader, A. Sorvina, P.V. Simpson, P.J. Wright, S. Stagni, S.E. Plush, M. Massi, D. A. Brooks, Imaging nuclear, endoplasmic reticulum and plasma membrane events in real time, FEBS Lett. 590 (2016) 3051–3060, https://doi.org/10.1002/1873-3468.12365.

[19] C.A. Bader, E.A. Carter, A. Safitri, P.V. Simpson, P.J. Wright, S. Stagni, M. Massi, P. A. Lay, D.A. Brooks, S.E. Plush, Unprecedented staining of polar lipids by a luminescent rhenium complex revealed by FTIR microspectroscopy in adipocytes, Mol. BioSyst. 12 (2016) 2064–2068, https://doi.org/10.1039/c6mb00242k.

[20] C.A. Bader, T. Shandala, E.A. Carter, A. Ivask, T. Guinan, S.M. Hickey, M. V. Werrett, P.J. Wright, P.V. Simpson, S. Stagni, N.H. Voelcker, P.A. Lay, M. Massi, S.E. Plush, D.A. Brooks, A molecular probe for the detection of polar lipids in live cells, PLoS One 11 (2016), https://doi.org/10.1371/journal.pone.0161557.

[21] V. Fiorini, A.M. Ranieri, S. Muzzioli, K.D.M. Magee, S. Zacchini, N. Akabar, A. Stefan, M.I. Ogden, M. Massi, S. Stagni, Targeting divalent metal cations with Re (I) tetrazolato complexes, Dalton Trans. 44 (2015) 20597–20608, https://doi.org/10.1039/c5dt03690a.

[22] M.V. Werrett, P.J. Wright, P.V. Simpson, P. Raiteri, B.W. Skelton, S. Stagni, A. G. Buckley, P.J. Rigby, M. Massi, Rhenium tetrazolato complexes coordinated to thioalkyl-functionalised phenanthroline ligands: synthesis, photophysical characterisation, and incubation in live HeLa cells, Dalton Trans. 44 (2015) 20636–20647, https://doi.org/10.1039/c5dt03470a.

[23] T. Topala, A. Bodoki, L. Oprean, R. Oprean, Bovine Serum Albumin Interaction with metal complexes, Clujul Medical 87 (2014) 215–219.

[24] T. Peters, Serum albumin, Adv. Protein Chem. 37 (1985) 161–245, https://doi.org/10.1016/S0065-3233(08)60065-0.

[25] D. Peak, T.C. Werner, R.M. Dennin, J.K. Baird, Fluorescence quenching at high quencher concentrations, J. Chem. Phys. 79 (1983) 3328, https://doi.org/10.1063/1.446234.

[26] H. Boaz, G.K. Rollefson, The quenching of fluorescence. Deviations from the Stern-Volmer Law, J. Am. Chem. Soc. 72 (1950) 3435–3443, https://doi.org/10.1021/ja01164a032.

[27] J. Keizer, Nonlinear fluorescence quenching and the origin of positive curvature in Stern-Volmer plots, J. Am. Chem. Soc. 105 (1983) 1494–1498, https://doi.org/10.1021/ja00344a013.

[28] J.R. Lakowicz "Principles of Fluorescence Spectroscopy, 3rd ed." Plenum: New York, 2006. DOI:10.1007/978-0-387-46312-4.

[29] K.M. Danielsen, Y.-P. Chin, J.S. Buterbaugh, T.L. Gustafson, S.J. Traina, Solubility enhancement and fluorescence quenching of pyrene by humic substances: the effect of dissolved oxygen on quenching processes, Environ. Sci. Technol. 29 (1995) 2162–2165, https://doi.org/10.1021/es00008a042.

[30] W.R. Ware, Oxygen quenching of fluorescence in solution: an experimental study of the diffusion process, J. Phys. Chem. 66 (1962) 455, https://doi.org/10.1021/j100809a020.

[31] C.-Y. Gao, X. Qiao, Z.-Y. Ma, Z.-G. Wang, J. Lu, J.-L. Tian, J.-Y. Xu, S.-P. Yan, Synthesis, characterization, DNA binding and cleavage, BSA interaction and anticancer activity of dinuclear zinc complexes, Dalton Trans. 41 (2012) 12220–12232, https://doi.org/10.1039/C2DT31306E.

[32] G. Scatchard, The attraction of proteins for small molecules and ions, Ann. N.Y. Acad. Sci. 51 (1949) 660, https://doi.org/10.1111/j.1749-6632.1949.tb27297.x.

[33] N. Ghosh, R. Mondal, S. Mukherjee, Inverse temperature dependence in static quenching versus calorimetric exploration: binding interaction of chloramphenicol to β-lactoglobulin, Langmuir 29 (2015) 8074–8080, https://doi.org/10.1021/acs.langmuir.5b02103.

[34] M. van de Weert, L. Stella, Fluorescence quenching and ligand binding: a critical discussion of a popular methodology, J. Mol. Struct. 998 (2011) 144–150, https://doi.org/10.1016/j.molstruc.2011.05.023.

[35] V. Rajendiran, R. Karthik, M. Palaniandavar, H. Stoeckli-Evans, V.S. Periasamy, M. A. Akbarsha, B.S. Srinag, H. Krishnamurthy, Mixed-ligand copper(II)-phenolate complexes: effect of coligand on enhanced DNA and protein binding, DNA cleavage, and anticancer activity, Inorg. Chem. 46 (2007) 8208–8221, https://doi.org/10.1021/ic700755p.

[36] G.A. Crosby, J.N. Demas, Measurement of photoluminescence quantum yields. Review, J. Phys. Chem. 75 (1971) 991–1024, https://doi.org/10.1021/j100678a001.
[37] F. Eaton, Reference materials for luminescence measurements, Pure Appl. Chem. 60 (1988) 1107–1114.
[38] K. Nakamaru, Synthesis, luminescence quantum yields, and lifetimes of trischelated ruthenium(II) mixed-ligand complexes including 3,3′-dimethyl-2,2′-bipyridyl, Bull. Chem. Soc. Jpn. 55 (1982) 2697–2705, https://doi.org/10.1246/bcsj.55.2697.
[39] K. Koguro, T. Oga, S. Mitsui, R. Orita, Novel synthesis of 5-substituted tetrazoles from nitriles, Synthesis (1998) 910–914, https://doi.org/10.1055/s-1998-2081.
[40] N. Monti, S. Zacchini, M. Massi, A. Hochkoeppler, L. Giorgini, V. Fiorini, A. Stefan, S. Stagni, Antibacterial activity of a new class of tris homoleptic Ru(II)-complexes with alkyl-tetrazoles as diimine-type ligands, Appl. Organomet. Chem. 34 (2020), https://doi.org/10.1002/aoc.5806.
[41] G.M. Sheldrick, SADABS-2008/1 - Bruker AXS Area Detector Scaling and Absorption Correction, Bruker AXS, Madison, Wisconsin, USA, 2008.
[42] G.M. Sheldrick, Crystal structure refinement with SHELXL – IUCr, Acta Crystallogr. C 71 (2015) 3, https://doi.org/10.1107/S2053229614024218.